PERGAMON

International Journal of Rock Mechanics and Mining Sciences 36 (1999) 361–380

International Journal of
Rock Mechanics
and Mining Sciences

Quantifying progressive pre-peak brittle fracture damage in rock during uniaxial compression

E. Eberhardt[a,*], D. Stead[b], B. Stimpson[c]

[a]*Engineering Geology, Swiss Federal Institute of Technology Zürich, ETH Hönggerberg, 8093 Zurich, Switzerland*
[b]*Camborne School of Mines, University of Exeter, Cornwall TR15 3SE, UK*
[c]*Department of Civil and Geological Engineering, University of Manitoba, Winnipeg, Man., Canada R3T 5V6*

Accepted 8 January 1999

Abstract

This paper presents the findings of an extensive laboratory investigation into the identification and quantification of stress-induced brittle fracture damage in rock. By integrating the use of strain gauge measurements and acoustic emission monitoring, a rigorous methodology has been developed to aid in the identification and characterization of brittle fracture processes induced through uniaxial compressive loading. Results derived from monocyclic loading tests demonstrate that damage and the subsequent deformation characteristics of the damaged rock can be easily quantified by normalizing the stresses and strains observed in progression from one stage of crack development to another. Results of this analysis show that the crack initiation, σ_{ci}, and crack damage, σ_{cd}, thresholds for pink Lac du Bonnet granite occur at $0.39\sigma_{UCS}$ and $0.75\sigma_{UCS}$, respectively. Acoustic emissions from these tests were found to provide a direct measure of the rapid release of energy associated with damage-related mechanisms. Simplified models describing the loss of cohesion and the subsequent development of microfractures leading up to unstable crack propagation were derived using normalized acoustic emission rates. Damage-controlled cyclic loading tests were subsequently used to examine the effects of accumulating fracture damage and its influence on altering the deformation characteristics of the rock. These tests revealed that two distinct failure processes involving the progressive development of the microfracture network, may occur depending on whether the applied cyclic loads exceed or are restrained by the crack damage stress threshold.

1. Introduction

Canada's concept for the permanent disposal of nuclear fuel waste proposes that a disposal facility be located at a depth of 500 to 1000 m in the plutonic rock of the Canadian Shield [1]. Some of the key concerns regarding the design of the facility include the implications of potential ground disturbance by the excavation method and the redistribution of in situ stresses around the excavation. Both of these factors relate to the extent of brittle fracture damage which could adversely affect the stability of the excavation boundary and could increase the permeability of the near-field host rock.

These concerns, however, are not restricted to the design of nuclear waste repositories. Although a disposal vault is a unique underground facility, the design, excavation and construction of the facility is similar to that required for many other major underground engineering projects (for example, transportation tunnels). Stability analysis for these openings, in cases where discontinuities play an insignificant factor, typically involves a comparison between the state of stress surrounding the excavation and the intact strength of the host rock. If redistribution of stresses following excavation results in a critical imbalance in the energy of the system, then the progressive degradation of the rock mass strength through stress-induced brittle fracturing may ensue.

* Corresponding author. Tel.: +41-1-633-2594; fax: +41-1-633-1108.
E-mail address: erik@erdw.ethz.ch (E. Eberhardt)

0148-9062/99/$ - see front matter
PII: S0148-9062(99)00019-4

Work at Atomic Energy of Canada Limited's Underground Research Laboratory (URL) has concentrated on quantifying rock damage through the identification of stress-induced crack generation [2–4]. Martin [2] showed that areas of high tangential compressive stresses near the tunnel face significantly contribute to the strength degradation of the rock through brittle fracturing. Observations of in situ behaviour at the URL suggest that strength degradation begins with the initiation of the microfracturing process, termed crack initiation, σ_{ci}, and can end in failure at stresses well below the uniaxial compressive strength, σ_{UCS}, of the material. Martin [2] and Read et al. [5] identified a crack damage stress threshold, σ_{cd} ($<\sigma_{UCS}$) and equated this to the long term strength. Thus, the identification of these processes and their associated mechanisms are of key interest in predicting both the short- and long-term stability of an excavation. This paper presents the findings from two extensive series of laboratory tests directed towards identifying and quantifying the effects of stress-induced brittle fracture damage during uniaxial compression.

2. Quantifying damage in rock

Munson et al. [6] and Martin and Read [7] have observed that the microfracturing process can be correlated to the progressive failure of a circular opening in brittle rock. In general, microfractures contribute to the failure process by locally altering the mechanical properties of the material. The propagation of a microfracture can be equated with the irreversible destruction of molecular cohesion along the generated fracture path. In this sense, the microfracturing process acts to 'damage' the material. As the number of propagating fractures multiply, damage can be viewed as accumulative and can be correlated to observed decreases in the elastic stiffness and cohesive strength of the material (Refs. [8,9], respectively). Rock deformation between fracture initiation and failure, therefore, can be attributed to the continuous accumulation of stress-induced fracture damage.

The notion of fracture damage and the quantification of its effects on the mechanical properties of a material has developed into a field of study known as damage mechanics. Mazars and Pijaudier-Cabot [10] define damage mechanics as the description of the local effects of microfracturing and the evolution of the mechanical properties of the continuum as microfractures develop. These effects include elastic stiffness degradation, induced anisotropy, anelastic strains and cohesion loss. The theory of damage, therefore, describes the evolution of material behaviour between the virgin state and the fracture-induced failed state. Damage mechanics acts to quantify these changes by introducing a continuous internal state variable called the 'damage', which may be regarded as a continuous measure of the state of internal degradation of the stiffness of the material considered [11].

The concept of a continuous measure of damage has been used extensively to describe various types of failure in metals and other types of solids. Lemaitre and Chaboche [12] review these damage models which include damage formulation based on ductile plastic, creep and fatigue failures. Singh and Digby [11] review a number of similar damage relationships developed for brittle materials. In each of these cases, the effects of microfracturing are quantified through the development of a damage variable within a constitutive equation which, in turn, acts to describe the degradation of elastic stiffness for a given material. One of the simplest of these relationships, the uniaxial linear elastic damage law, can be written as:

$$\varepsilon_e = \frac{\sigma}{(1-D)E} \tag{1}$$

where

ε_e = elastic uniaxial strain
σ = uniaxial stress
D = damage
E = elastic or Young's modulus

Although this model assumes all material behaviour (i.e. elasticity, plasticity, viscoplasticity) is affected in the same way by damage defects, the formulation provides a coherent and efficient stress–strain relationship [12].

The measurements required for these formulations have for the most part involved the coupling of deformation with damage. Shao and Khazraei [13] have demonstrated that laboratory stress–strain data can be used to both establish the required damage parameters and to calibrate the derived damage models. The versatility of laboratory stress–strain data is also demonstrated through its ability to measure a wide range of rock behaviour. This has allowed for the development of damage models for such complex behaviour as creep deformation in rocksalt [6,14] and subcritical crack growth [15]. To a lesser extent, the development and calibration of damage models have also been achieved using acoustic emission [16,17].

The quantification of microfracturing damage has proven to be a valuable consideration in the design of underground openings. The application of a damage criterion allows for the practical implementation of fracture processes derived through laboratory experiments. Simple relationships such as those proposed by Martin and Read [7] can be used to correlate the microfracturing process observed in laboratory tests to the extent and characteristics of the damaged zone sur-

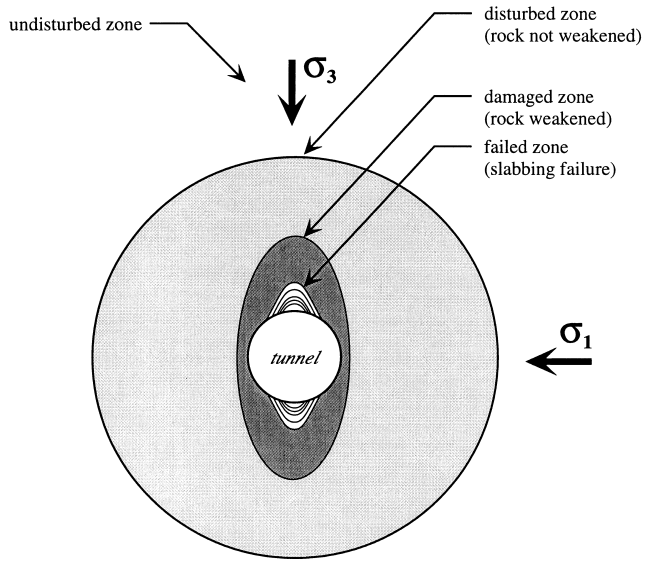

Fig. 1. Characteristics and extent of the disturbed and damaged zone surrounding a tunnel in a plane perpendicular to the tunnel axis (after Ref. [7]).

rounding an underground excavation in brittle rock (Fig. 1). Establishing the parameters associated with the initiation and propagation of microfractures, however, has proven difficult as existing methods based on laboratory testing incorporate a high degree of error and subjectivity [8]. Uncertainties also exist with respect to the mechanisms acting during the microfracturing process and how these processes contribute to the progressive degradation of material strength. These issues are addressed in Section 3.

3. Experimental procedures and interpretation of laboratory test data

Based on laboratory studies involving the stress–strain behaviour of brittle rock [18,19], the failure process can be broken down into a number of stages characterized by changes in the measured axial and lateral strain response recorded during uniaxial and triaxial compression tests (Fig. 2). These stages include:

1. Crack closure.
2. Linear elastic deformation.
3. Crack initiation and stable crack growth.
4. Crack damage and unstable crack growth.
5. Failure and post peak behaviour.

Crack closure, σ_{cc}, occurs during the initial stages of loading when existing cracks orientated at an angle to the applied load close. During crack closure, the stress–strain response is non-linear, exhibiting an increase in axial stiffness. Once the majority of existing cracks have closed, linear elastic deformation takes place. Crack initiation, σ_{ci}, represents the stress level where microfracturing begins. The growth of these cracks has been shown to occur in the direction of the

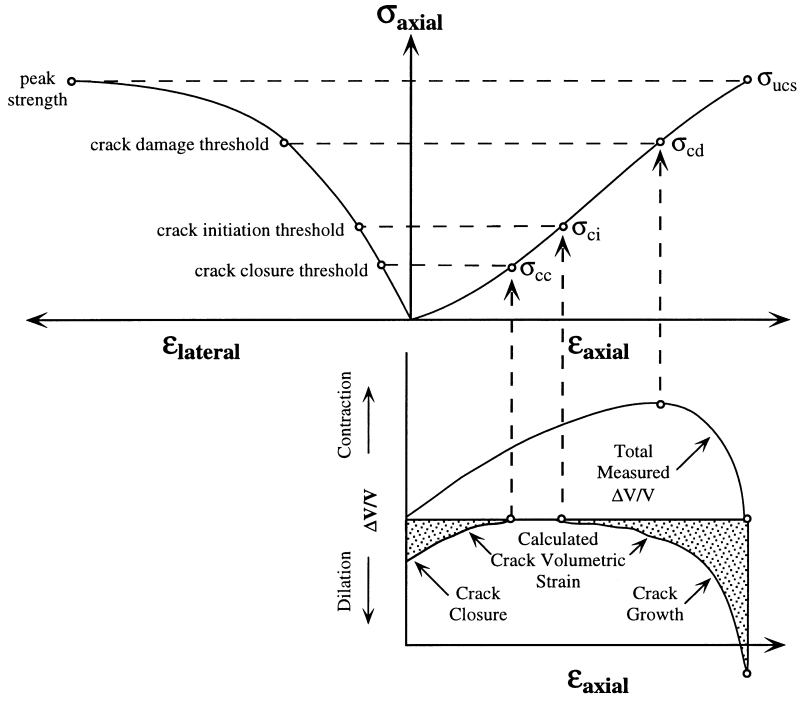

Fig. 2. Stress–strain diagram showing the stages of crack development (after Ref. [2]). Note that the axial and lateral strains are measured and the volumetric and crack volumetric strains are calculated.

major principal stress, σ_1, so that cracks not aligned with σ_1 grow along a curved path to align themselves with σ_1 [20–23]. The opening of cracks with faces parallel to the applied load are therefore detected as a departure from linear lateral and volumetric strain behaviour. Crack propagation is either stable or unstable. Under stable conditions, crack growth can be stopped by controlling the applied load. Unstable crack growth, also referred to as the crack damage stress threshold, σ_{cd}, has been associated with the point of reversal in the total volumetric strain curve (Fig. 2) and is the condition at which the relationship between the applied stress and the crack length ceases to exist and other parameters, such as the crack growth velocity, take control of the propagation process [19]. Under such conditions, crack propagation will continue until failure even if the applied loading is held constant.

Studies at the URL have focussed on using the crack initiation (σ_{ci}) and crack damage (σ_{cd}) stress thresholds to better quantify the in situ state of damage surrounding tunnel excavations. Confidently establishing these thresholds through laboratory testing, however, proved difficult especially with respect to crack initiation. It was found that methods based on the calculation of the crack volume, as described by Martin and Chandler [9] and Hatzor and Palchik [24], were limited due to their dependence on the use of the elastic constants E and ν. Eberhardt [4] has shown that although the Young's modulus, E, for Lac du Bonnet granite can be determined with a reasonably high degree of confidence and consistency, the non-linearity of the lateral strain response complicates the determination of Poisson's ratio, ν. This non-linearity introduces a large degree of uncertainty into the crack volume calculation used to determine the crack initiation threshold. Other methods based on visual inspection of the lateral and volumetric strain curves (e.g. Lajtai and Dzik [25]) were found to be even more limited due to poor data resolution and subjectivity in interpreting the results.

Table 1
Average crack threshold values for pink Lac du Bonnet granite (standard deviation in parentheses)

Threshold parameter	Value (MPa)
Number of tests	20
Crack closure, σ_{cc}	47.3 ($\pm$2.7)
Crack initiation, σ_{ci}	81.5 ($\pm$3.7)
Secondary cracking, σ_{ci2}	103.9 ($\pm$5.0)
Crack coalescence, σ_{cs}	132.8 ($\pm$9.0)
Crack damage, σ_{cd}	156.0 ($\pm$13.2)
Peak strength, σ_{UCS}	206.9 ($\pm$13.5)

Eberhardt et al. [8] found that crack initiation threshold values could be more accurately determined using an approach that combined the use of acoustic emission event counts with a moving point regression analysis performed on uniaxial stress–strain data. These threshold values were further confirmed through measured changes in other AE event properties such as the ringdown count, event duration, rise time [26] and the elastic impulse 'energy' rate [8]. These techniques also led to the delineation of two additional crack thresholds which mark the initiation of cracking within the stronger quartz grains of the Lac du Bonnet granite, termed the secondary crack initiation threshold, σ_{ci2}, and a threshold marking the beginning

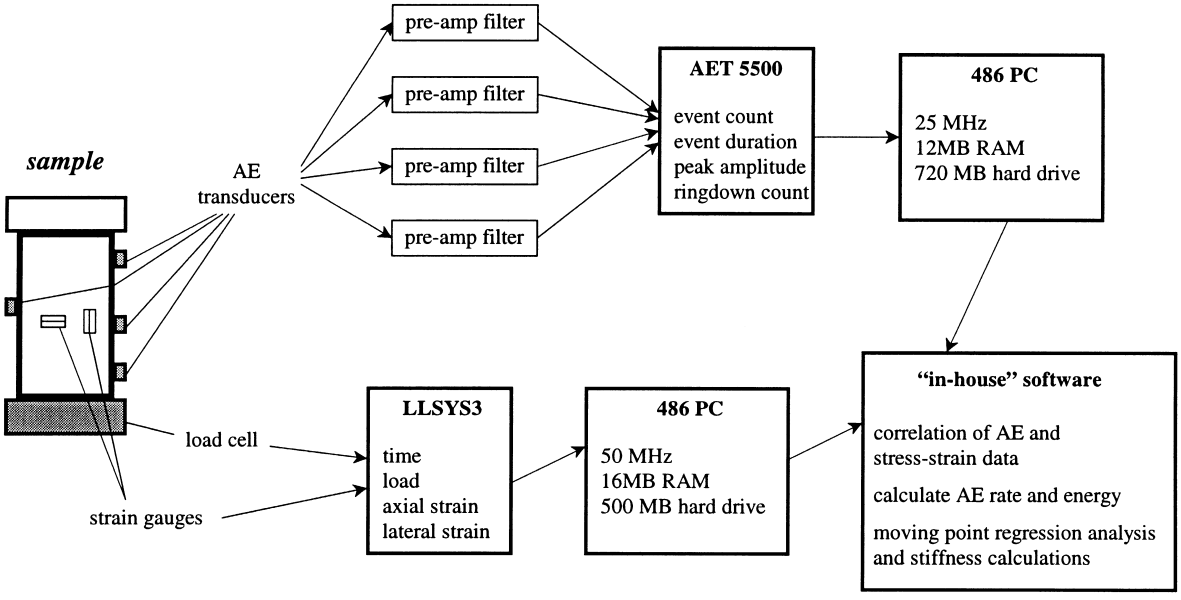

Fig. 3. Schematic of strain gauge and acoustic emission instrumentation, and data collection systems.

Table 2
Crack thresholds normalized with respect to uniaxial compressive strength for pink Lac du Bonnet granite (standard deviation in parentheses)

Crack threshold	Normalized relationship
Number of tests	10
Crack closure, σ_{cc}	$0.23\sigma_{UCS}$ ($\pm$0.02)
Crack initiation, σ_{ci}	$0.39\sigma_{UCS}$ ($\pm$0.03)
Secondary cracking, σ_{ci2}	$0.51\sigma_{UCS}$ ($\pm$0.03)
Crack coalescence, σ_{cs}	$0.65\sigma_{UCS}$ ($\pm$0.04)
Crack damage, σ_{cd}	$0.75\sigma_{UCS}$ ($\pm$0.05)

of crack interaction and coalescence, termed the crack coalescence threshold, σ_{cs}. The different threshold points for pink Lac du Bonnet granite are shown in Table 1.

4. Simple damage relationships derived from uniaxial compression tests

Results from a series of 10 uniaxial compression tests were examined in order to quantify the state of microfracturing damage with respect to stress, strain and acoustic emission properties. Testing was conducted at the University of Saskatchewan's Rock Mechanics Laboratory on cylindrical samples of pink Lac du Bonnet granite obtained from the 130 m level of the URL (i.e. 130 m below ground surface). Samples were prepared for testing according to ASTM standards with length to diameter ratios of approximately 2.25 and were instrumented with six electric resistance strain gauges (3 axial and 3 lateral at 60° intervals, 12.7 mm in length, with a 5% strain limit) and four 175 kHz resonant frequency, piezoelectric AE transducers. Uniaxial loading was applied to the samples at a constant rate of 0.25 MPa/s so that failure occurred between 5 and 10 min as recommended by the ISRM [27]. Applied loads and the resulting strains were recorded using an automatic data acquisition system, sampling at an average rate of 2–3 readings per second, thereby overcoming any deficiencies in data resolution. The AE monitoring system consisted of a bandpass filter with a frequency range of 125 kHz to 1 MHz and a pre-amplifier with 40 dB total gain and a dynamic range of 85 dB. The AE data was recorded with an AET 5500 monitoring system using a threshold value of 0.1 V. A schematic of the testing system used is provided in Fig. 3.

4.1. Normalized stresses and strains

A method available to quantify damage induced through uniaxial compression is to normalize the stresses and strains required to pass from one stage of crack development to another. Table 2 shows the relationship between axial stress, normalized with respect to the uniaxial compressive strength, σ_{UCS}, and the different stages of crack development for the pink Lac du Bonnet granite. The system of normalizing stress values for the crack initiation and crack damage thresholds has been widely used at the URL. Martin [28] reported values of 0.3–0.4 σ_{UCS} for the crack initiation threshold, σ_{ci}, and 0.7 σ_{UCS} for the crack damage threshold, σ_{cd}. These values correspond to those presented in Table 2. Standard deviations for the normalized values were seen to be relatively small, although increased standard deviations were recorded with increasing stress levels Table 1, likely relating to a degree of randomness in the crack propagation process.

Test results were also analyzed to determine the proportioning of axial and lateral strains between threshold intervals. Results shown in Table 3 reveal that approximately 30% of the total axial strain occurred during crack closure and nearly half occurred before any cracking was detected. In contrast, only 7% of the total lateral strains were recorded during the crack closure interval thus demonstrating that crack closure predominantly involves cracks preferentially aligned perpendicular to the applied load. The largest proportion of total lateral strain, approximately 66%, was seen to be attributable to the coalescence and unstable propagation of growing cracks (Fig. 4).

Normalized strains can also be used in the development of simple constitutive relationships for application in analytical, empirical or numerical models. In

Table 3
Axial and lateral strains, corresponding to the stages of crack development, normalized with respect to the maximum strains recorded at failure for pink Lac du Bonnet granite (standard deviation in parentheses)

Crack threshold	Normalized axial strain	Normalized lateral strain
Number of tests	10	10
Crack closure, σ_{cc}	$0.33\varepsilon_{ax\_max}$ ($\pm$0.04)	$0.07\varepsilon_{lat\_max}$ ($\pm$0.01)
Crack initiation, σ_{ci}	$0.45\varepsilon_{ax\_max}$ ($\pm$0.04)	$0.16\varepsilon_{lat\_max}$ ($\pm$0.03)
Secondary cracking, σ_{ci2}	$0.55\varepsilon_{ax\_max}$ ($\pm$0.05)	$0.23\varepsilon_{lat\_max}$ ($\pm$0.04)
Crack coalescence, σ_{cs}	$0.68\varepsilon_{ax\_max}$ ($\pm$0.05)	$0.34\varepsilon_{lat\_max}$ ($\pm$0.05)
Crack damage, σ_{cd}	$0.77\varepsilon_{ax\_max}$ ($\pm$0.05)	$0.44\varepsilon_{lat\_max}$ ($\pm$0.07)

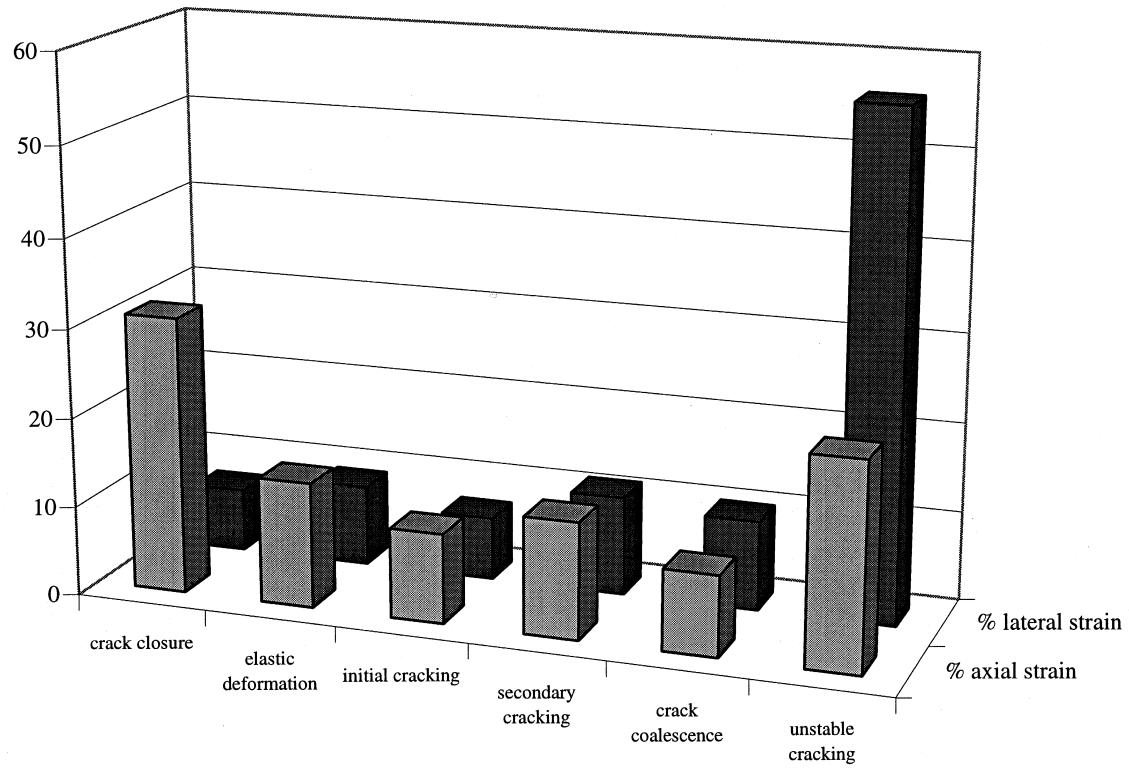

Fig. 4. Percentage of total strains associated with each stage of crack development for pink Lac du Bonnet granite.

some cases specialized numerical codes such as FLAC [29], allow the formulation of subroutines through which normalized values can be used to dictate the modelled material behaviour. Table 4 defines the deformation process for Lac du Bonnet granite in terms of the variation in the axial deformation modulus, E_{def}, and the ratio of lateral to axial deformation, ν_{def}. It should be noted that unlike the elastic constants, E and ν, these parameters combine linear and non-linear strains accumulated within the given stress interval. These deformation parameters can subsequently be incorporated into numerical models allowing for more realistic simulations in terms of changes in material behaviour with progressive microfracturing. Fig. 5 illustrates the fit of the modelled deformation parameters to the normalized stress–strain curve derived from a uniaxial compression test performed on a pink Lac du Bonnet granite sample. One advantage of using a simple design methodology such as this is that once the deformation parameters are determined the model provides a quick approximation of the material behaviour. However, this simple methodology only addresses the deformation characteristics of the rock observed in the laboratory, it does not address the loss of cohesion and material strength associated with progressive microfracturing.

Table 4
Deformation parameters for pink Lac du Bonnet granite in terms of the axial deformation modulus, E_{def}, and the ratio of the lateral to axial strains, ν_{def}

Stress interval	E_{def} (GPa)	ν_{def}
Number of tests	10	10
Crack closure (0 to σ_{cc})	42.2	0.09
Elastic deformation (σ_{cc} to σ_{ci})	63.8	0.23
Stable cracking I (σ_{ci} to σ_{ci2})	65.6	0.29
Stable cracking II (σ_{ci2} to σ_{cs})	64.7	0.34
Crack coalescence (σ_{cs} to σ_{cd})	62.8	0.45
Unstable cracking (σ_{cd} to σ_{UCS})	60.8	1.01

4.2. Normalized acoustic emission

Normalized strain gauge measurements provide a simple means to describe the deformation characteristics of samples during the progressive accumulation of microfracturing damage. These measurements include the plastic strains associated with crack development, as well as elastic strains and plastic strains associated with the deformation of constituent minerals. The direct correlation of these strains to the loss of cohesion, however, becomes somewhat more difficult. Acoustic emissions, on the other hand, provide a direct measure of discrete damage events in brittle material such as pore collapse, crack propagation and grain boundary movements [30].

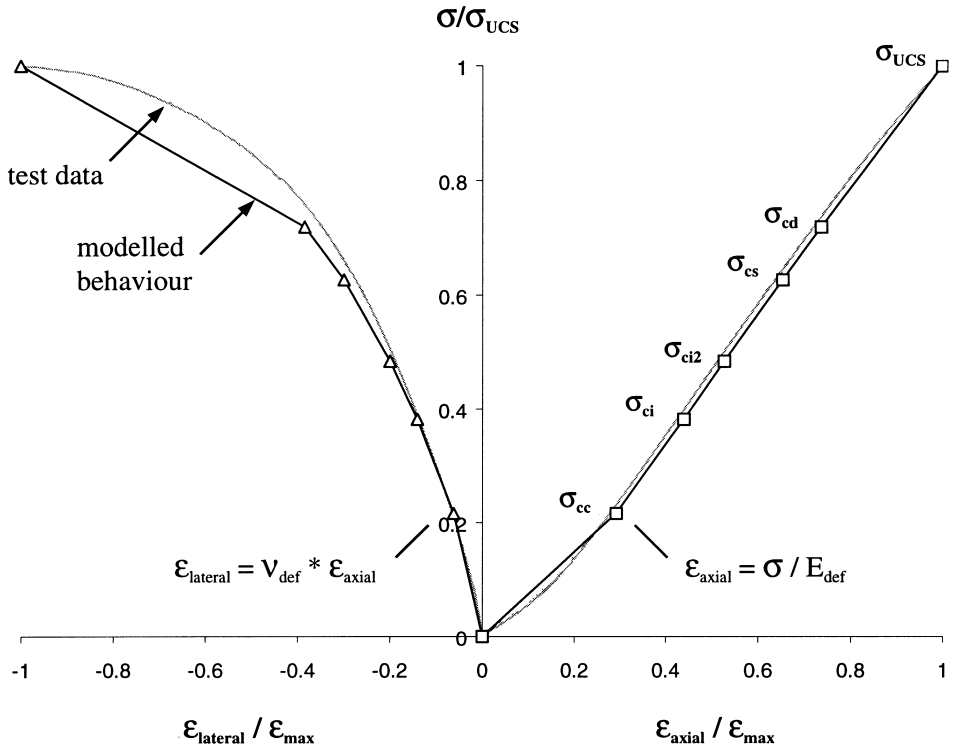

Fig. 5. Uniaxial stress versus strain plot for pink Lac du Bonnet granite comparing laboratory test data to modelled behaviour presented in Table 4.

Acoustic emission data was analyzed to develop a simple relationship between AE activity and the gradual loss of cohesion and the accumulation of damage. Total AE event counts up to each crack threshold were normalized with respect to the total number of events recorded at failure so that comparisons could be made between individual tests. This procedure was necessary since a number of factors can cause variations in the sensitivity of the AE transducers from test to test. For example, the degree of coupling achieved between the sample and the transducers can have a significant effect on the total number of events recorded. The AE detection sensitivity can also be physically controlled through adjustments to the gain and detection threshold. Several settings were tested before being finalized (these values were presented earlier). It was found that the relative proportion of events recorded between the different thresholds of crack development remained fairly constant regardless of the AE detection sensitivity. One exception to this observation was with respect to the number of events recorded during the crack closure interval. Lower detection threshold values (i.e. increased sensitivity) resulted in higher event counts during crack closure. This was likely due to the increased sensitivity to lower energy events associated with the mechanisms acting during crack closure. To correct for this, events recorded during crack closure were subtracted from the total cumulative count. Thus, events 'recognized' up to the crack initiation threshold include only those recorded after crack closure.

AE counts were also normalized with respect to the total number of events recorded at the crack damage threshold, σ_{cd}, since a high number of events were recorded during unstable crack propagation leading up to failure. Results from the analysis of event counts are presented in Table 5. Assuming that the number of AE events detected up to ultimate failure can be directly correlated to damage, it may be inferred that the majority of damage-causing mechanisms occur during unstable crack propagation (approximately 83%). However, if it assumed that once crack propagation becomes unstable and failure, therefore, appears

Table 5
Cumulative AE event count, normalized with respect to the total events at peak strength and the crack damage threshold, for pink Lac du Bonnet granite (standard deviation in parentheses)

Crack threshold	AE/(AE at σ_{peak})	AE/AE at σ_{cd})
Number of tests	5	10
Crack initiation, σ_{ci}	$0.006AE_{total}$ (±0.002)	$0.063AE_{total}$ (±0.041)
Secondary cracking, σ_{ci2}	$0.024AE_{total}$ (±0.011)	$0.185AE_{total}$ (±0.084)
Crack coalescence, σ_{cs}	$0.094AE_{total}$ (±0.031)	$0.552AE_{total}$ (±0.090)
Crack damage, σ_{cd}	$0.175AE_{total}$ (±0.024)	$1.000AE_{total}$ (±0.000)
Peak strength, σ_{UCS}	$1.000AE_{total}$ (±0.000)	n/a

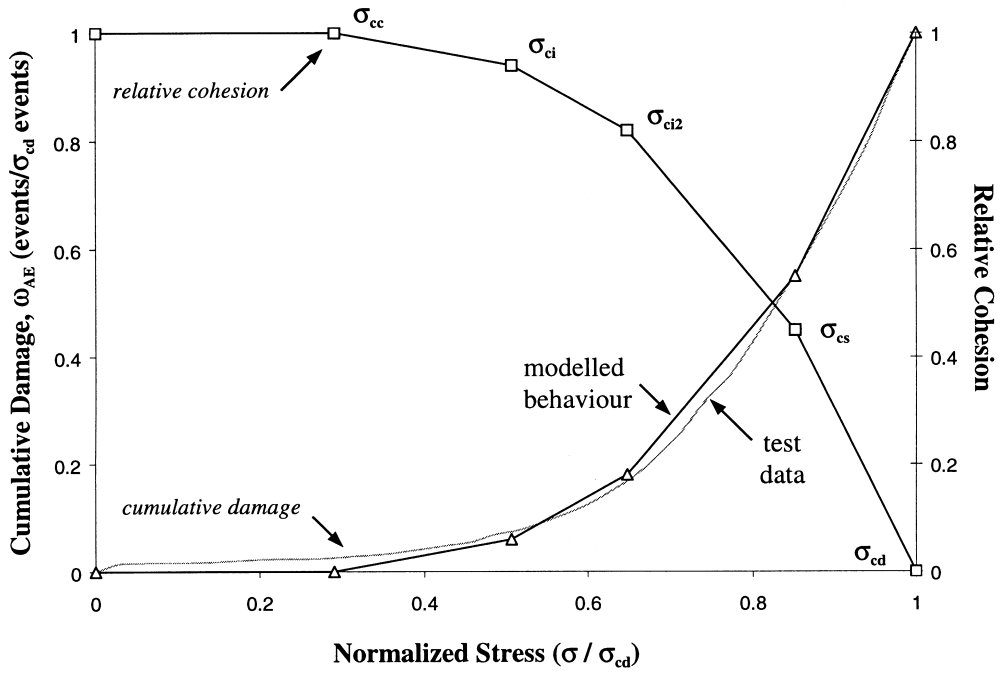

Fig. 6. Plots of normalized damage and relative cohesion versus normalized axial stress from AE event counts for pink Lac du Bonnet granite.

to be inevitable, then the data can be normalized with respect to σ_{cd} Table 5. From this respect, approximately 55% of the damage-causing mechanisms leading up to unstable crack propagation occur prior to crack coalescence and 45% afterwards. Using these values, it is possible to develop simplified criteria which describe the accumulation of damage (gradual loss of cohesion) resulting in the brittle failure of the sample.

It is possible to use the values shown in Table 5 to construct a simplified model describing the damage or loss of cohesion leading up to unstable crack propagation. Fig. 6 demonstrates the fit of the model to test data for the Lac du Bonnet granite and also shows the progressive loss of cohesion as a function of the normalized AE damage. It is also possible to fit a third order polynomial to the test data which would allow for the direct incorporation of a continuous function describing the accumulation of AE detected damage throughout loading. Derived with respect to mean values for the ten tests this function can be written as:

$$\omega_{AE} = \frac{\sigma}{\sigma_{cd}}\left(\frac{2.2\sigma^2}{\sigma_{cd}^2} - \frac{1.5\sigma}{\sigma_{cd}} + 0.3\right) \quad (2)$$

where

ω_{AE} = acoustic emission cumulative damage parameter (AE count/total AE count at σ_{cd})

σ_{cd} = crack damage threshold (MPa)

σ = axial stress (MPa)

The *r*-squared value (i.e. R^2) for the fit of this expression to the experimental data is 0.9995. A similar relationship can be derived to include the acoustic events recorded between the crack damage and peak strength thresholds (i.e. normalizing the cumulative AE count with respect to the total number of events recorded at failure). However, due to the sharp increase in the number of events recorded just prior to failure a good fit can only be obtained using a sixth order polynomial. This essentially renders the relationship intractable due to the increased complexity required to describe the entire damage curve. The simplified relationship derived with respect to the crack damage threshold Eq. (2) is thus more practical.

The simplest application of a damage criterion based on AE events would likely be in the form of a failure criterion incorporated into a numerical model and would allow direct comparison between modelled stresses and the degree of induced microfracturing damage. It would also be possible to implement these relationships in a constitutive model that allows for plastic deformation with increasing damage. The obvious deficiency of these simplified models, however, is that they are derived from laboratory-based uniaxial compression tests. Further study would be required to determine the sensitivity of these models to confining stresses, thus taking into account the true nature of the stress state surrounding an underground opening.

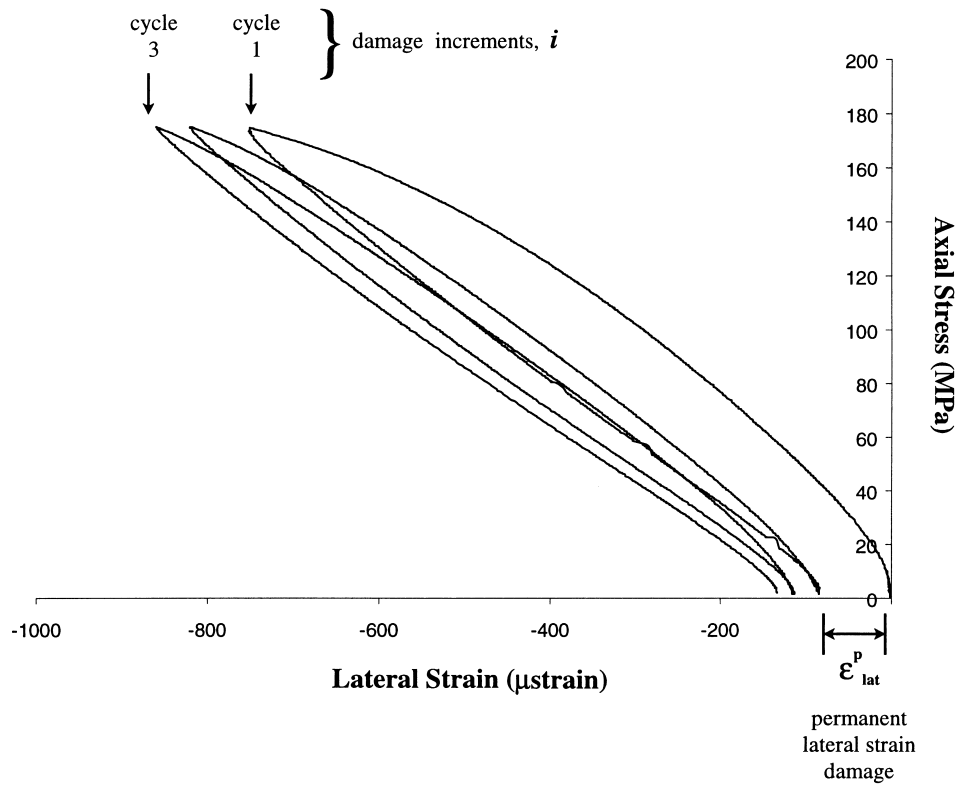

Fig. 7. Axial stress versus lateral strain showing the first three cycles of a cyclic loading test and the resulting permanent lateral strain damage, ε^{p}_{lat}, with respect to the damage increment, i.

5. Damage-control cyclic loading tests

The relationships previously described characterize the effects of microfracturing damage induced through single stage loading in uniaxial compression tests. However, the stress history of the near field rock surrounding an underground opening is more complex. For example, Martin [2] has shown that the state of stress at a point ahead of the tunnel face can increase, unload and then increase again as the tunnel advances towards and passes the point. If these stresses induce microfracturing but not failure, then the mechanical properties of the rock may vary significantly from point to point depending on the local stress history. These loading and unloading cycles ahead of the face may damage the rock to a level where it fails when exposed in the tunnel well below the undamaged strength values for the rock.

Martin and Chandler [9] performed a series of cyclic loading tests, termed damage-control tests, to correlate increasing damage to changes in cohesion and the mobilization of friction. In the development of these relationships, cohesion was equated to the crack damage threshold, σ_{cd}, for each cycle normalized with respect to the peak strength of the rock. The friction angle was similarly related to the σ_{cd} under the assumption that friction was mobilized at this point. These tests, however, primarily concentrated on loading conditions which would allow the test to be carried on into the post-failure region of the stress–strain curve. They were also limited to strain gauge measurements (i.e. no acoustic emission measurements).

To further investigate the role of cyclic loading in contributing to damage, a series of cyclic loading tests were performed in which the various stages of crack development presented in the first part of this study were measured in combination with the detection of acoustic emissions. In these tests, damage was defined in terms of the permanent axial, lateral and volumetric strains (ω_{ax}, ω_{lat} and ω_{vol}, respectively), in addition to the recorded number of acoustic events, ω_{AE}. It should be noted that a separate analysis of both the permanent axial and lateral strain parameters was undertaken, as opposed to limiting the analysis to volumetric strain. This allowed for differentiation between permanent strains resulting from either the initiation and opening of cracks, primarily detected through lateral strain measurements, or the closure or coalescence of cracks, primarily detected through axial strain measurements [8]. For each case, the damage measured over a single load–unload cycle, or damage increment 'i' (Fig. 7), was normalized with respect to the total damage measured throughout the test. These parameters are thus defined as follows:

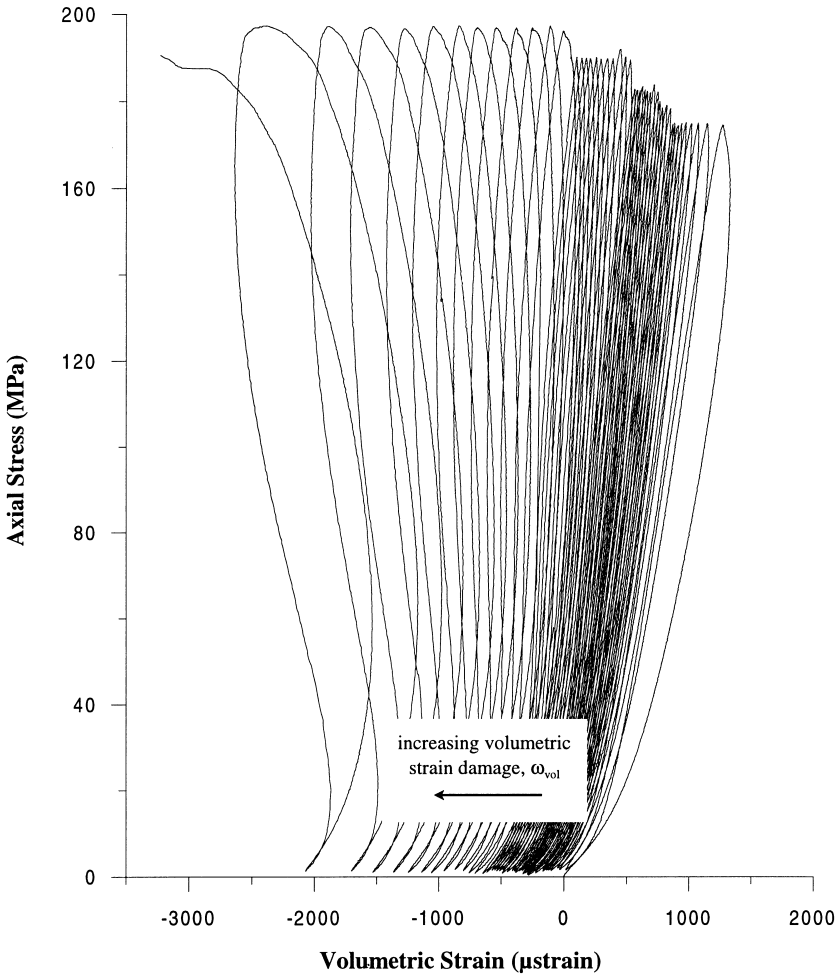

Fig. 8. Axial stress versus volumetric strain showing the migration of the volumetric strain curve with each damage increment.

$$\omega_{ax} = \frac{(\varepsilon^{p}_{ax})_i}{\sum_{i=1}^{n}(\varepsilon^{p}_{ax})_i} \quad (3)$$

$$\omega_{lat} = \frac{(\varepsilon^{p}_{lat})_i}{\sum_{i=1}^{n}(\varepsilon^{p}_{lat})_i} \quad (4)$$

$$\omega_{vol} = \frac{(\varepsilon^{p}_{vol})_i}{\sum_{i=1}^{n}(\varepsilon^{p}_{vol})_i} \quad (5)$$

$$\omega_{AE} = \frac{(N)_i}{\sum_{i=1}^{n}(N)_i} \quad (6)$$

where

ω_{ax}, ω_{lat}, ω_{vol} and ω_{AE}	= damage parameters
ε^{p}_{ax}, ε^{p}_{lat} and ε^{p}_{vol}	= permanent strain
N	= number of recorded AE events
i	= damage increment (i.e. one load–unload cycle)

Relationships derived from these parameters were tested and analyzed for two different load histories: (i) cyclic loads which *exceeded* the crack damage threshold with each damage increment and (ii) cyclic loads restricted to stresses just *below* the crack damage threshold.

5.1. Damage-control testing above the crack damage threshold

In the first damage-control test, a sample of pink Lac du Bonnet granite was loaded in uniaxial compression to a stress level above σ_{cd} (approximately 180 MPa). The sample was then unloaded, completing one

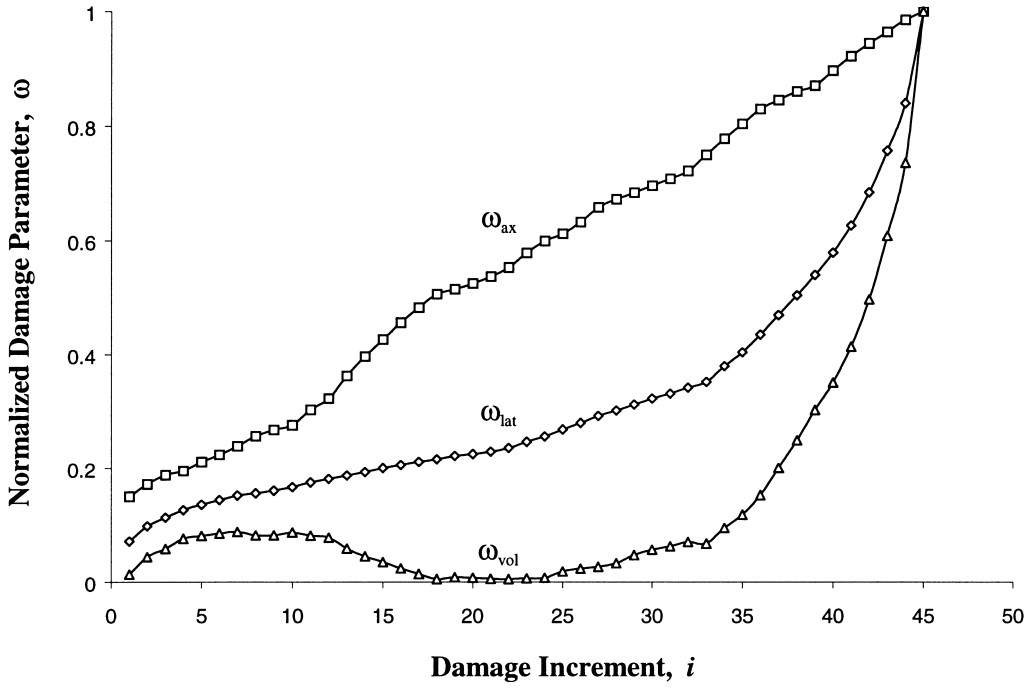

Fig. 9. Normalized axial (ω_{ax}), lateral (ω_{lat}) and volumetric (ω_{vol}) strain damage versus damage increment for pink Lac du Bonnet granite.

damage increment, and then reloaded. This process was repeated until the sample failed at damage increment $i=46$ (i.e. 46 cycles). Load rates for these cycles were approximately 25 to 30 MPa/min with the test taking approximately 8 h to complete. In general, the test procedure closely followed that described by Martin and Chandler [9] with the exception that the test was not carried into the post peak region. Fig. 8 shows that with each damage increment, permanent volumetric strains accumulated in the sample and comprised both the axial and the lateral strain damage components (Fig. 9). It should be noted that there was an apparent decrease in the volumetric strain damage between 10 and 20 cycles (Fig. 9), even though increasing damage was recorded in both the axial and lateral directions. This result is an artifact of the volumetric

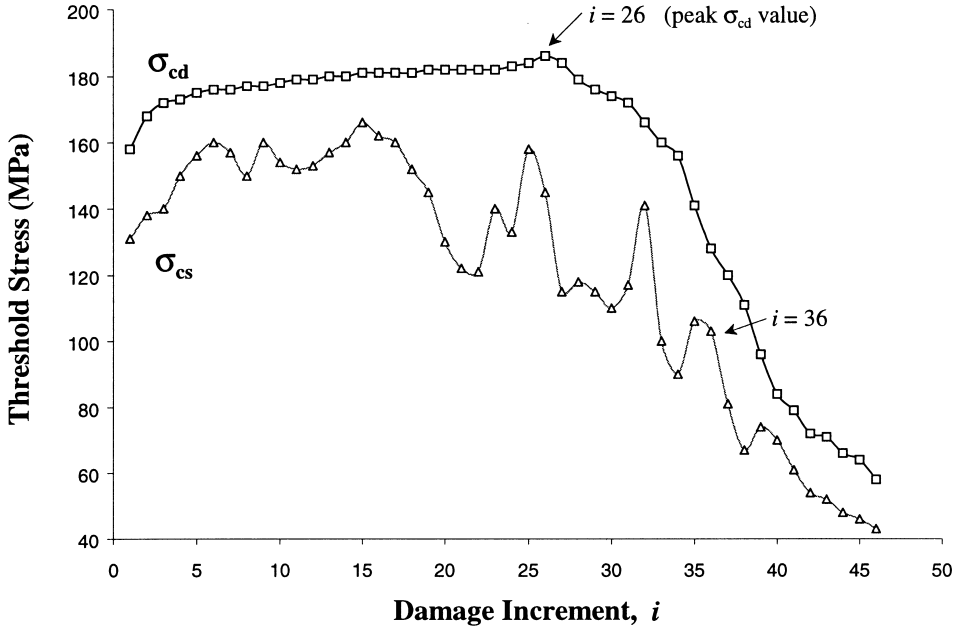

Fig. 10. Crack damage, σ_{cd}, and crack coalescence, σ_{cs}, threshold stresses versus damage increments for pink Lac du Bonnet granite.

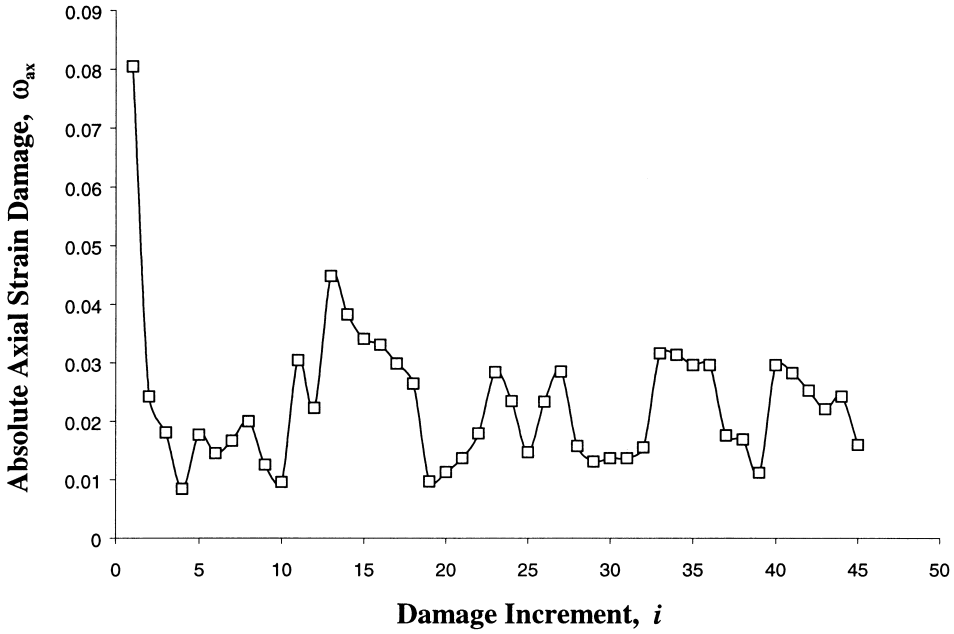

Fig. 11. Absolute axial strain damage versus damage increment showing the axial damage induced for each load–unload cycle normalized with respect to the total damage at failure for pink Lac du Bonnet granite.

strain calculation for small strains in a cylinder based on the axial and lateral strain (i.e. $\varepsilon_{vol} = \varepsilon_{ax} + 2\varepsilon_{lat}$).

In terms of material behaviour, increases in damage over a number of load and unload cycles were seen to progressively reduce the strength of the rock as measured by the crack damage threshold. Fig. 10 shows that σ_{cd} for the sample slowly increased up to damage increment $i = 26$ before rapidly dropping to values well below the initial crack initiation threshold, σ_{ci}, for the rock. Values for the crack coalescence threshold, σ_{cs}, followed a similar pattern with the exception that small-scale fluctuations occurred throughout the test. These oscillations reflected similar oscillations in the absolute axial strain damage (Fig. 11) and likely reflect the build-up and release of localized energy as cracks coalesce. Fig. 12 illustrates these possible mechanisms in which the coalescence of interacting cracks would be accompanied by large plastic strains as the bridging material between the cracks weakens and collapses. The coalescence of smaller cracks would result in the development of new, effectively longer cracks in which the crack tip would be located in less damaged material and therefore stiffer material. Increased load (i.e. stresses) would be required during the next damage increment to develop the process zone around the tips of these newly formed cracks, i.e. σ_{cs} would increase. This process may repeat itself during subsequent load–unload cycles. These increases in the crack coalescence threshold, however, only occur over short intervals of one or two damage increments; the decreasing trend of the curve (Fig. 10) indicates a general degradation of strength.

The progressive accumulation of damage in the sample also resulted in the degradation of stiffness. Young's modulus, E, and Poisson's ratio, ν, were calculated for each cycle by assuming linearity between the crack closure and crack damage thresholds. Fig. 13 shows that through the first 25 damage increments, changes in E and ν show a gradual softening of the rock sample. In general, Poisson's ratio over these damage increments increased at a greater rate than the Young's modulus values decreased. This would seem to indicate that the predominant mechanism throughout these cycles is the steady growth of axial cracks. At damage increments 26 and 37, however, increases in Poisson's ratio values were seen and were followed by decreases in the Young's modulus. It is interesting to note that damage increment 26 coincides with the peak crack damage threshold shown in Fig. 10 and both damage increments 26 and 37 approximately coincide with decreases in the crack coalescence threshold.

Examination of the state of damage at increment 26 suggests a correlation between the crack damage threshold and cohesion. Fig. 14 shows that when broken down into its individual strain components, the permanent damage induced is unequally shared. In terms of the lateral strain damage parameter, ω_{lat}, only 30% of the permanent lateral strains occurs before the peak crack damage threshold is reached at damage increment 26. In contrast, over 60% of the axial strain damage was induced prior to this point. Presumably, during the loading history of the sample, the state of crack development reaches a critical point

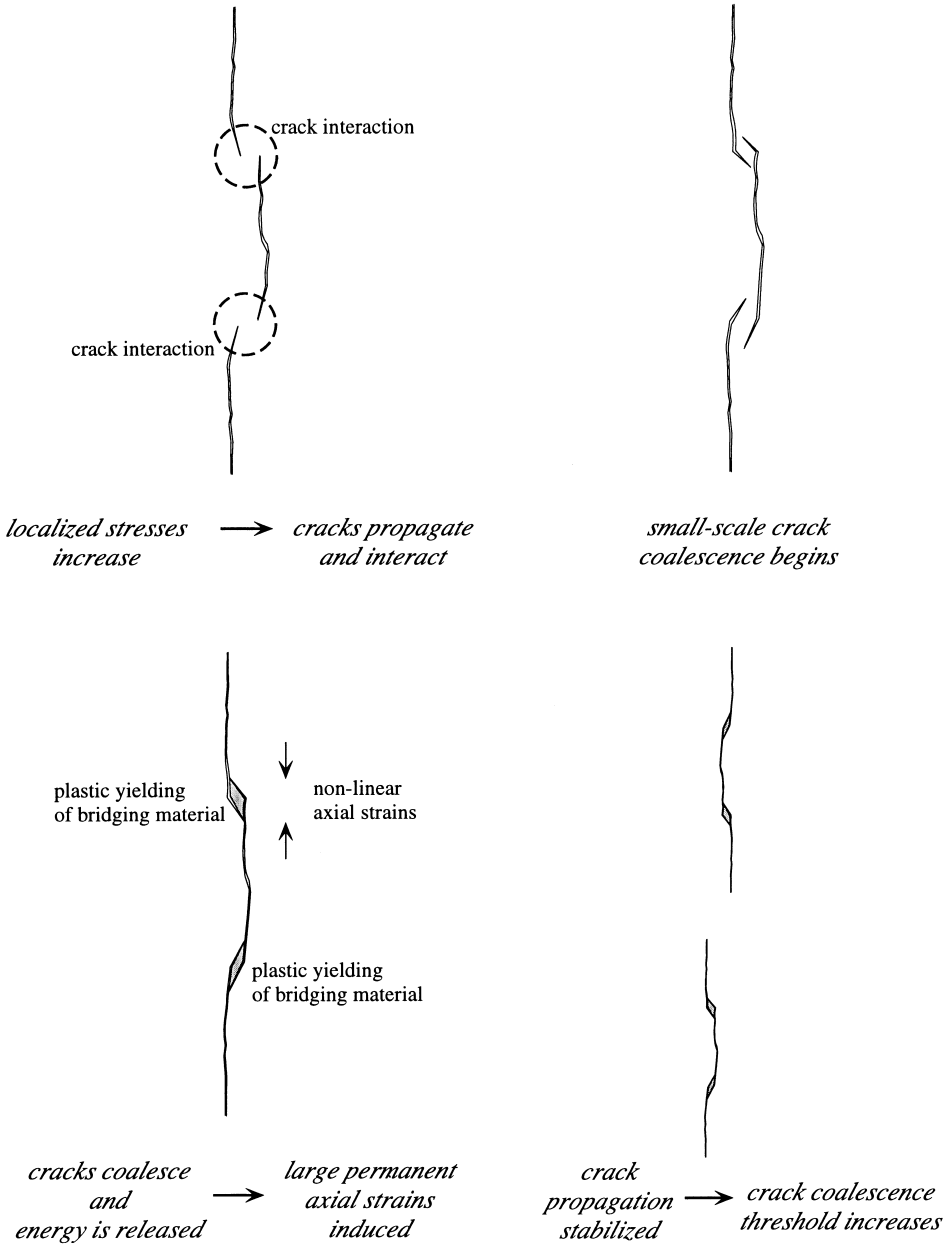

Fig. 12. Conceptual model of crack coalescence accompanied by large permanent axial strains (i.e. axial strain damage).

beyond which further damage results in an increasing rate of loss of cohesion in the sample. The magnitude of induced axial damage prior to this critical point, relative to lateral damage, suggests that crack interaction and coalescence plays a much larger part in the development of significant damage than does the initiation of new cracks.

The influence crack interaction and coalescence have on the crack damage level can be assessed by relating data from the damage-control test to data from the uniaxial compression tests. In the latter, the initiation of fractures in the Lac du Bonnet granite began at approximately 40% of the peak strength or 82 MPa Table 1. Continuous cracking associated with the secondary initiation of fractures in quartz grains (i.e. σ_{ci2}) was detected at 50% of peak strength or 102 MPa. These values agree with those determined for the first cycle of the damage-control test (82 and 106 MPa, respectively). It is postulated that for the first damage increment, a population of cracks was initiated which subsequently propagated and coalesced on a local level but without reaching an advanced state of coalescence as would be expected under prolonged unstable crack propagation conditions. Upon the second, third and ensuing load increments, the initiation of new fractures is expected to be minimal but the propagation of exist-

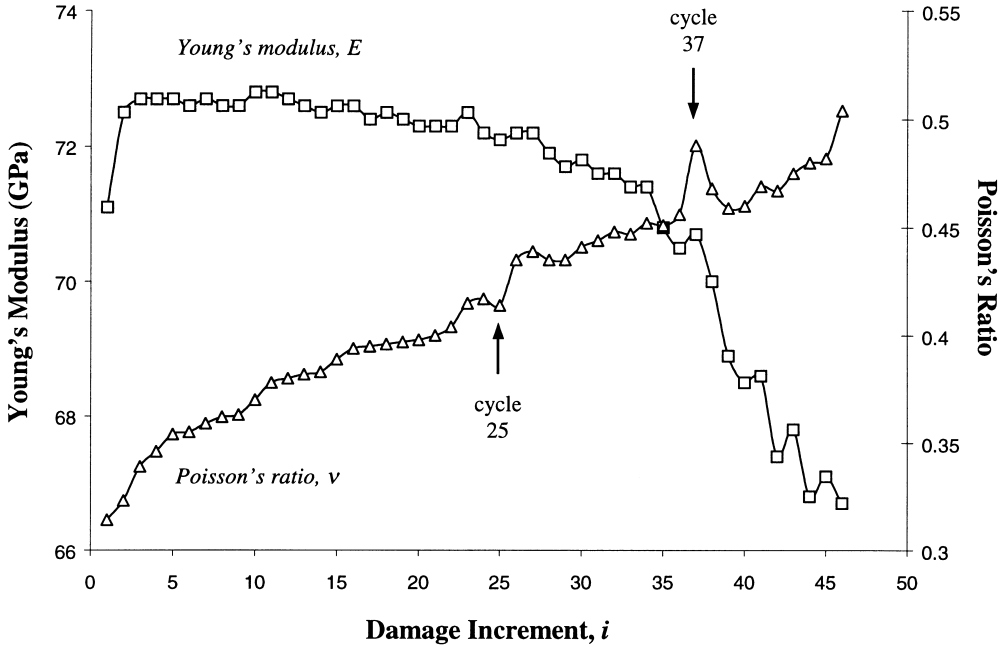

Fig. 13. Plots of Young's modulus and Poisson's ratio versus cyclic damage increments for pink Lac du Bonnet granite.

ing fractures would be extensive. AE event counts and observations from the damage-control test confirm these hypotheses. In each of the cycles following the first cycle, no new AE events were detected until the crack coalescence value from the first cycle was reached. Furthermore, significant cracking in these cycles wasn't detected until the crack damage threshold from the first cycle was reached (Fig. 15).

It would appear that with each damage increment, new cracking is limited but at stresses above σ_{cs} exist-

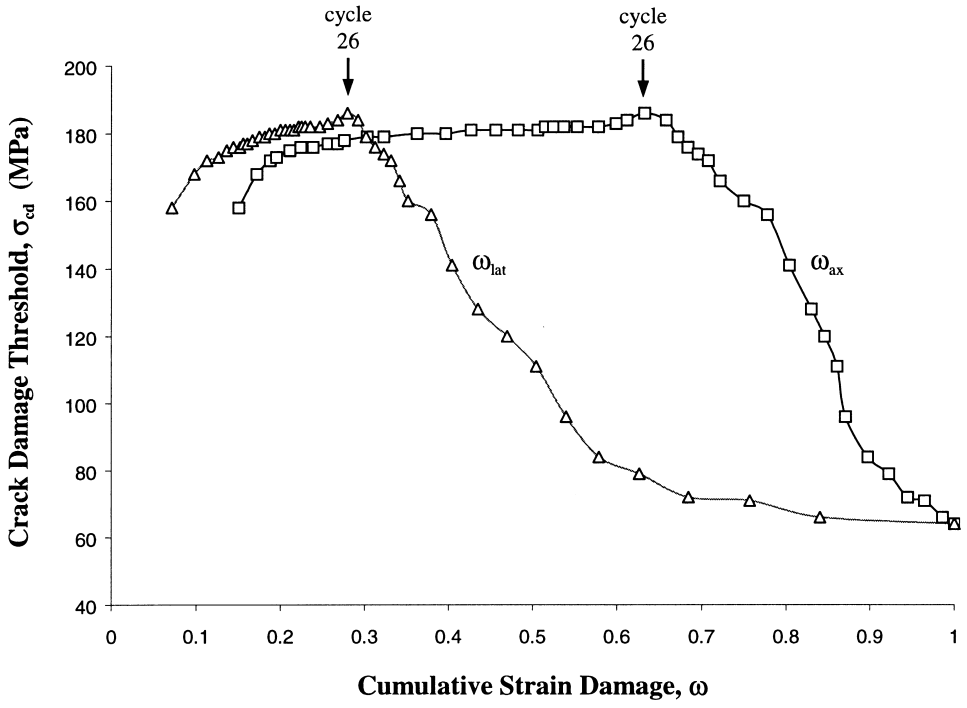

Fig. 14. Crack damage threshold recorded for each damage increment versus axial and lateral cumulative strain damage for pink Lac du Bonnet granite.

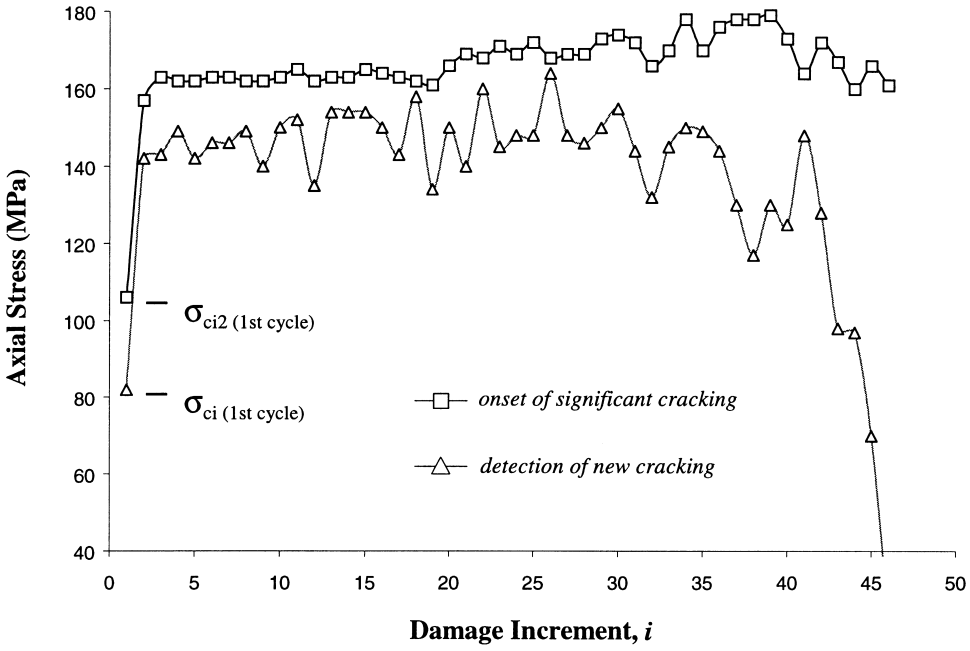

Fig. 15. Axial stress versus damage increments showing the stress levels at which new and significant cracking was detected through AE monitoring of pink Lac du Bonnet granite.

ing cracks reactivate, propagate and coalesce. The history of axial damage also suggests that the weakening and breakdown of bridging material between these cracks at higher stresses contributes to a significant proportion of the recorded plastic strain. These observations conform to those made through numerical modelling studies of crack tip interactions [31], in which cracks propagating in a uniaxial stress field were found to interact in such a fashion that the resulting crack population consisted of a relatively small number of long cracks as opposed to a large number of small cracks (as was found to be the case under triax-

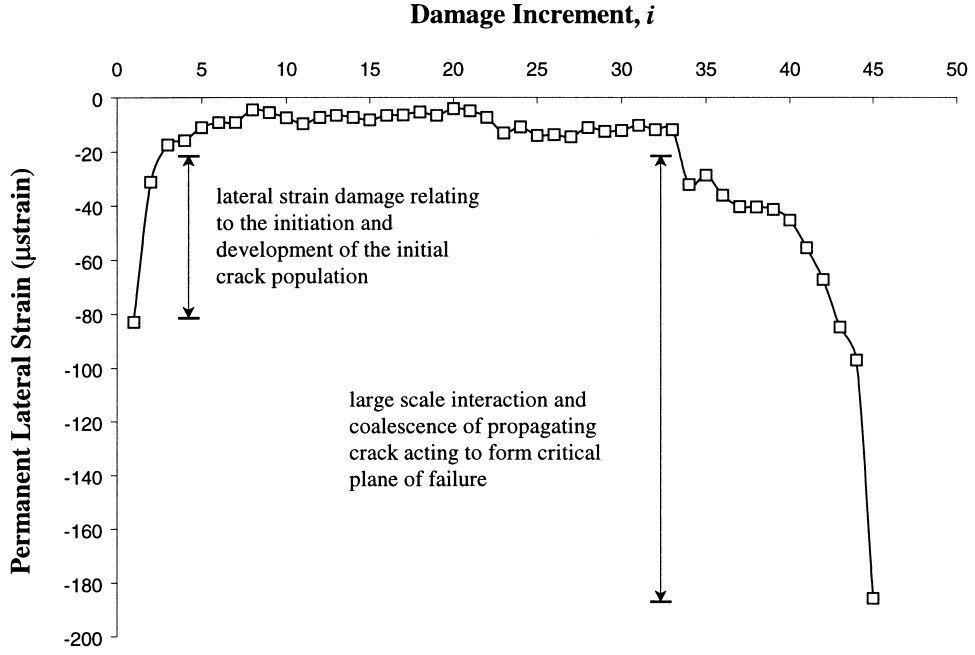

Fig. 16. Permanent lateral strain versus damage increments showing the lateral strain damage induced by each load–unload cycle for pink Lac du Bonnet granite.

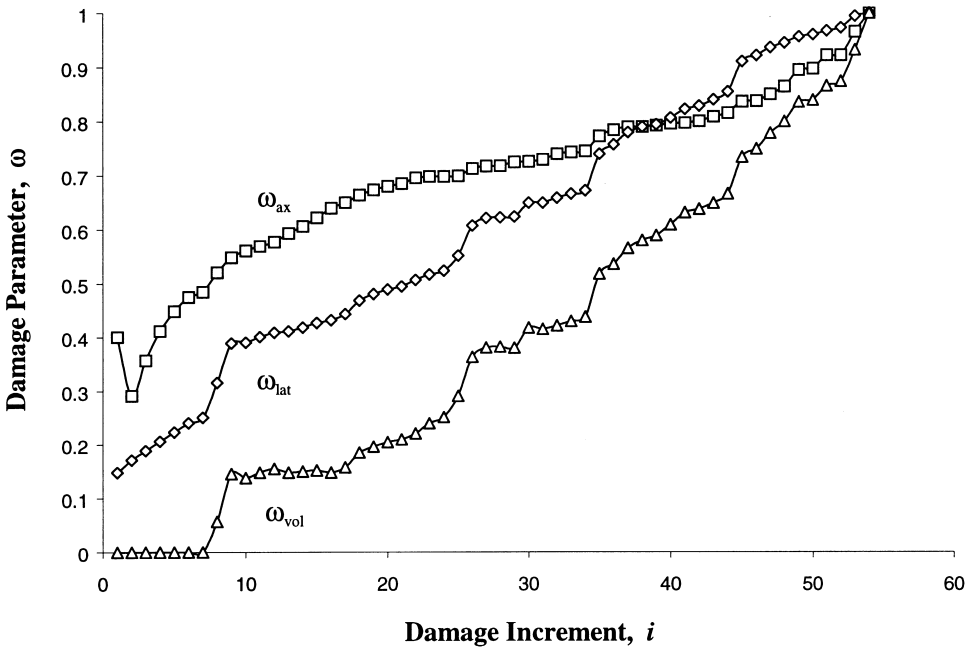

Fig. 17. Axial (ω_{ax}), lateral (ω_{lat}) and volumetric (ω_{vol}) strain damage versus damage increments for load cycling of pink Lac du Bonnet granite below the crack damage threshold.

ial loading conditions). Significant increases in lateral strain damage following the maximum σ_{cd} value suggests that the crack population reaches a state where cracks coalesce to form larger cracks which, in turn, coalesce until a critical plane is formed along which failure of the sample occurs (Fig. 16). It should be noted that although significant damage was induced in the sample in the cycles leading up to failure with reductions in cohesion and stiffness, failure still occurred in an explosive manner at a load of 196 MPa. The effects of microfracturing damage did not completely 'disaggregate' the granite so that it would fail in a plastic, soil-like manner. Instead, microfracturing acted to reduce the cohesion to a point whereby a series of unstable cracks could more readily form a critical plane along which failure occurred.

5.2. Damage-control testing below the crack damage threshold

In Section 5.1 it was shown that the crack damage threshold of the material rapidly decreased at the point where the lateral and axial strain damage parameters reached values of 0.29 and 0.67, respectively. These values closely match damage values determined for the crack coalescence threshold through monotonic loading (0.34 and 0.68, Table 3). It appears that the interaction and coalescence of propagating cracks plays a significant role in the degradation of material strength. This role was further explored through a second damage-control test. The setup and procedure for the test was identical to the first damage-control test with the exception that the maximum load for each damage increment was kept below the crack damage threshold. The test took 12 h to complete over which time 59 load–unload cycles were applied to the sample, pink Lac du Bonnet granite, before the sample failed. An average loading rate of 24 MPa/min was used.

Results from this test indicate that the behaviour of the sample was markedly different from that seen in the first damage-control test (where the maximum cyclic loads applied exceeded σ_{cd}). Although both the crack initiation and secondary crack thresholds were exceeded during the first cycle, the load was removed before the cracks reached an unstable propagation state (this was achieved through real-time monitoring of the AE event rate). It then appears that with each subsequent damage increment, both new cracks and existing cracks initiate and propagate. Fig. 17 shows the progressive accumulation of permanent strain damage measured throughout the test. Although the axial strain damage curve shows a steady rate of increase similar to that seen in the first test (Fig. 9), the lateral strain damage curve follows a different pattern. In the first test, a high degree of lateral strain damage was observed during the first cycle as new cracks initiated and propagated, followed by a relatively low amount of apparent damage in the subsequent cycles. The lateral strain damage curve maintained a low rate of increase even though loads exceeding the crack damage threshold were being applied. It wasn't until the lateral strain damage par-

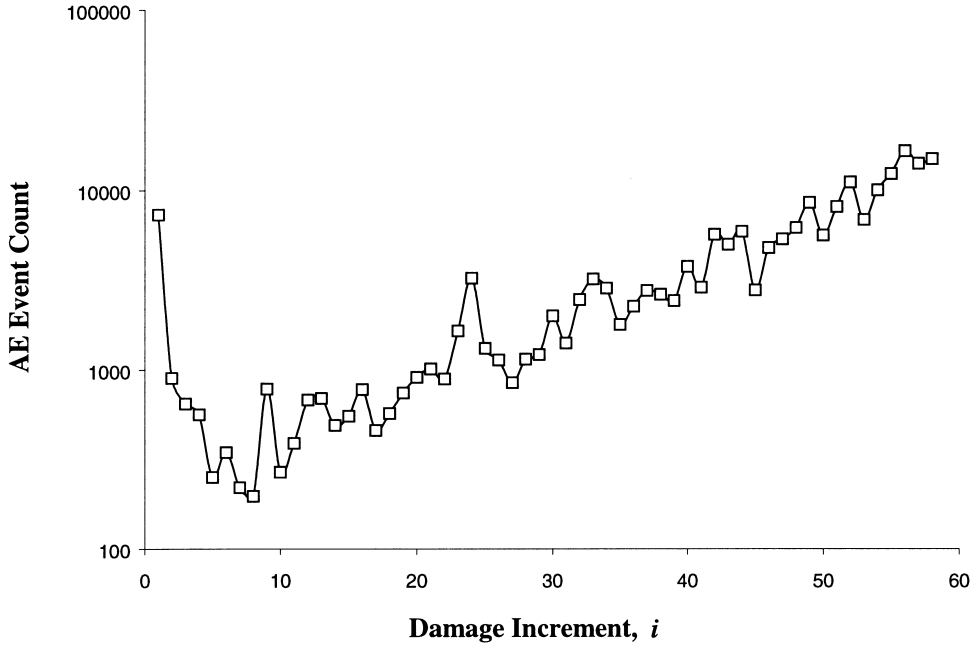

Fig. 18. Log plot of the AE event count versus damage increments for load cycling of pink Lac du Bonnet granite below the crack damage threshold.

ameter reached an approximate value of 0.3, at damage increment 33, that the rate of damage drastically increased (Figs. 9 and 16). In the second damage-control test (Fig. 17), the lateral strain damage curve was seen to follow a steady rate of increase throughout each cycle. Since lateral damage is indicative of the opening (i.e. initiation and propagation) of new cracks parallel to the direction of loading, it would appear that new cracks are generated with each damage increment.

These observations were validated through the AE event counts. Fig. 18 shows that a constantly increas-

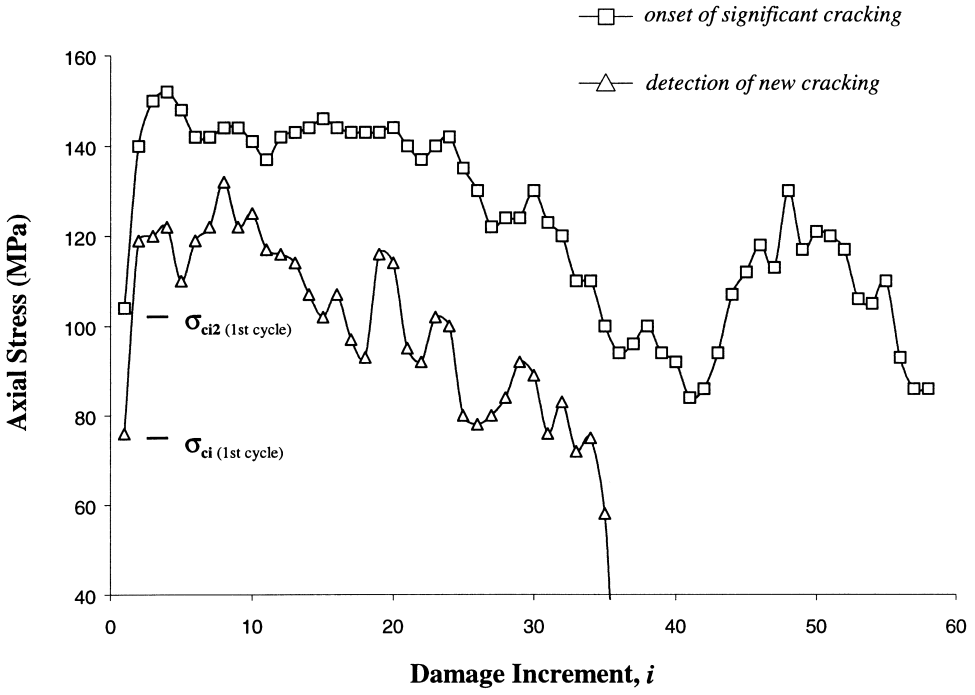

Fig. 19. Axial stress versus damage increments for load cycling of pink Lac du Bonnet granite below the crack damage threshold showing the stress levels at which new and significant cracking was detected through AE monitoring.

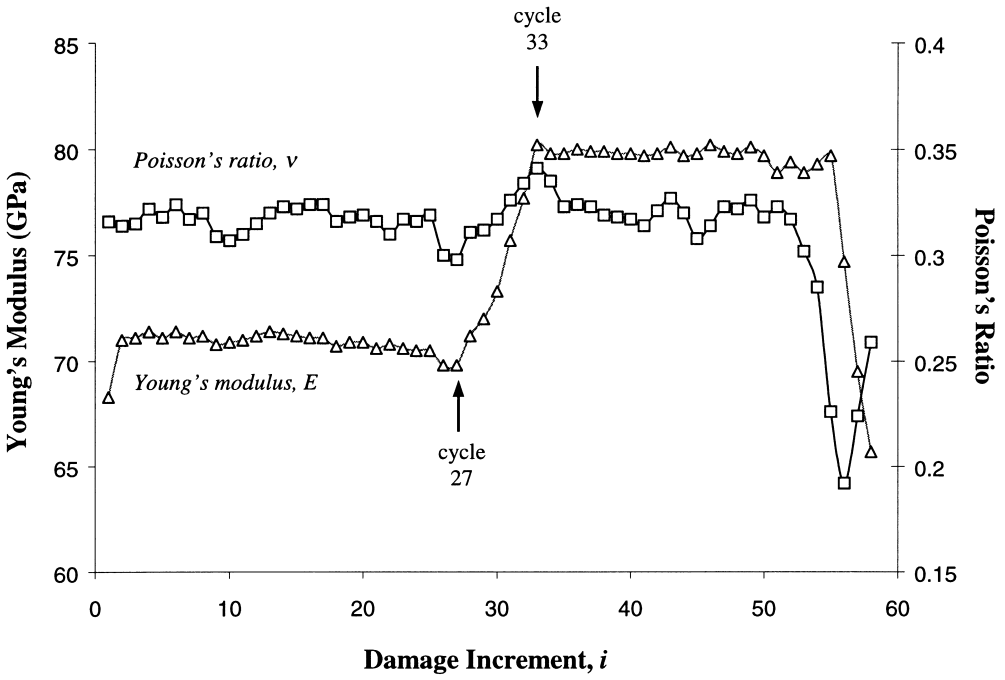

Fig. 20. Plots of Young's modulus and Poisson's ratio versus cyclic damage increments for load cycling of pink Lac du Bonnet granite below the crack damage threshold.

ing trend can be seen in the number of AE events detected with each damage increment. The plot also shows that damage increments with increased AE activity correlate to large increases in the lateral strain damage curve but not the axial strain damage curve. It was also observed that the loads at which significant AE events were detected generally decreased throughout most of the test (Fig. 19). In the first damage-control test with loading exceeding σ_{cd}, these values were seen to remain fairly constant (Fig. 15). This would seem to imply that with each damage increment a crack population of both new and existing cracks develops and grows. This pattern continued right up to failure at damage increment 59. Failure of the sample occurred in a brittle manner at a load of 110 MPa (approximately 0.5 σ_{UCS}), well below the crack damage threshold for undamaged Lac du Bonnet granite Table 1.

Limiting the damage increments to loads below the crack damage threshold was also seen to have a pronounced effect on the stiffness of the sample. Results from the first damage-control test showed that the deformation constants, E and ν, progressively decreased (Fig. 13). In contrast, the deformation constants calculated for the second damage-control test showed little change. Young's modulus and Poisson ratio values for this test remained fairly constant with each damage increment with the exception of a large jump in the Young's modulus between damage increments 27 and 33 (Fig. 20). This rapid increase in material stiffness suggests that some form of strain hardening may have occurred within the sample, possibly as angular asperities along coalesced crack faces locked-up.

These results suggest that by limiting the cyclic loads to stresses below the crack damage threshold, the degree of plastic yielding exhibited by bridging material (as depicted in Fig. 12) was greatly reduced. The breakdown of this material during crack coalescence and unstable crack propagation in the first test was seen to contribute to a large proportion of the plastic axial strains. It can thus be argued that significant internal breakdown in material stiffness does not occur until the crack population reaches a state, both in density and size, through which large scale crack interaction and coalescence can occur. This was not observed until the last four or five damage increments of the test (Fig. 20).

6. Summary and conclusions

A number of experimental approaches were explored in an effort to quantify stress-induced microfracturing damage observed in uniaxial compression tests. Test results demonstrated that damage and the deformation characteristics of the damaged material could be readily quantified by normalizing the stresses and strains required to pass from one stage of crack development to another. It was shown that crack initiation and crack damage for pink Lac du Bonnet granite

occur at $0.39\sigma_{UCS}$ and $0.75\sigma_{UCS}$, respectively. A damage dependent stress–strain relationship for the pink granite was determined using measurements of the axial deformation modulus, E_{def}, and the ratio of lateral to axial deformation, ν_{def}.

Acoustic emissions were found to provide a direct measure of the rapid release of energy associated with damage-related mechanisms. Simplified models describing the loss of cohesion and the subsequent development of microfractures leading up to unstable crack propagation were derived using normalized acoustic emission rates. Results indicate that approximately 55% of the damage-causing mechanisms leading up to unstable crack propagation occur prior to crack coalescence and 45% occur afterwards. A third order polynomial was found to describe the accumulation of damage leading up to unstable crack propagation.

Damage-controlled cyclic loading tests were used to examine the accumulation of damage and its influence on the deformation and fracture characteristics of granite samples. Several damage parameters were derived, permanent axial (ω_{ax}), lateral (ω_{lat}) and volumetric (ω_{vol}) strain, as well as the recorded number of acoustic events (ω_{AE}) induced with each damage increment (i). Results from the first of these damage-control tests, involving cyclic loads exceeding the crack damage threshold, showed that subsequent to the first damage increment very little new cracking occurred. Instead, existing cracks reactivated and propagated in an unstable fashion until the load was reduced. Results suggest that failure occurred through a process involving the coalescence of smaller cracks into larger cracks which, in turn, coalesced until a critical plane of failure was formed.

Results from the second damage-control test, in which cyclic loads were kept below the crack damage threshold, revealed that the slow development of the microcrack population resulted in the initiation and propagation of new cracks with each damage increment. Failure occurred when the crack population reached a state, both in density and size, through which large scale crack interaction, coalescence and unstable propagation ensued. This was marked by a large decrease in material stiffness over the last five damage increments of the test.

Acknowledgements

Parts of the work have been supported by Atomic Energy of Canada and an NSERC operating grant. The authors wish to thank Zig Szczepanik and Dr. Rod Read for their suggestions and contributions. Special thanks are extended to Dr. Emery Lajtai and Dr. Derek Martin for their insights into the initial stages of this work.

References

[1] Simmons GR, Baumgartner P. The disposal of Canada's nuclear fuel waste: engineering for a disposal facility. Pinawa: Whiteshell Laboratories, 1994 AECL-10715.

[2] Martin CD. Strength of massive Lac du Bonnet granite around underground openings. Ph.D. thesis, Department of Civil and Geological Engineering, University of Manitoba, Winnipeg, 1993.

[3] Read RS. Interpreting excavation-induced displacements around a tunnel in highly stressed granite. Ph.D. thesis, Department of Civil and Geological Engineering, University of Manitoba, Winnipeg, 1994.

[4] Eberhardt E. Brittle rock fracture and progressive damage in uniaxial compression. Ph.D. thesis, Department of Geological Sciences, University of Saskatchewan, Saskatoon, 1998.

[5] Read RS, Chandler NA, Dzik EJ. In situ strength criteria for tunnel design in highly-stressed rock masses. Int J Rock Mech Min Sci 1998;35(3):261–78.

[6] Munson DE, Holcomb DJ, DeVries KL, Brodsky NS, Chan KS. Correlation of theoretical calculations and experimental measurements of damage around a shaft in salt. In: Proceedings of the 35th US Symposium on Rock Mechanics, Reno. Rotterdam: A.A. Balkema, 1995. p. 491–6.

[7] Martin CD, Read RS. AECL's mine-by experiment: a test tunnel in brittle rock. In: Proceedings of the 2nd North American Rock Mechanics Symposium: Rock Mechanics Tools and Techniques, Montreal. Rotterdam: A.A. Balkema, 1996. p. 13–24.

[8] Eberhardt E, Stead D, Stimpson B, Read RS. Identifying crack initiation and propagation thresholds in brittle rock. Can Geotech J 1998;35(2):222–33.

[9] Martin CD, Chandler NA. The progressive fracture of Lac du Bonnet granite. Int J Rock Mech Min Sci Geomech Abstr 1994;31(6):643–59.

[10] Mazars J, Pijaudier-Cabot G. From damage to fracture mechanics and conversely: a combined approach. Int J Solids Struct 1996;33(20–22):3327–42.

[11] Singh UK, Digby PJ. A continuum damage model for simulation of the progressive failure of brittle rocks. Int J Solids Struct 1989;25(6):647–63.

[12] Lemaitre J, Chaboche J-L. Mechanics of solid materials. Cambridge: Cambridge University Press, 1990.

[13] Shao JF, Khazraei R. Wellbore stability analysis in brittle rocks with continuous damage model. In: Eurock '94: Rock Mechanics in Petroleum Engineering, Delft. Rotterdam: A.A. Balkema, 1994. p. 215–22.

[14] Aubertin M, Sgaoula J, Gill DE. A damage model for rocksalt: application to tertiary creep. In: 7th Symposium on Salt, Kyoto. Amsterdam: Elsevier Science Publishers, 1993. p. 117–25.

[15] Horii H, Okui Y. Micromechanics-based continuum theory and numerical analysis of localized phenomena. In: Proceedings of the 8th International Conference on Computer Methods and Advances in Geomechanics, Morgantown. Rotterdam: A.A. Balkema, 1994. p. 1687–92.

[16] Cox SJD, Meredith PG. Microcrack formation and material softening in rock measured by monitoring acoustic emissions. Int J Rock Mech Min Sci Geomech Abstr 1993;30(1):11–24.

[17] Shah KR, Labuz JF. Damage mechanisms in stressed rock from acoustic emission. J Geophys Res 1995;100(B8):15527–39.

[18] Brace WF. Brittle fracture of rocks. In: State of Stress in the Earth's Crust: Proceedings of the International Conference, Santa Monica. New York: American Elsevier Publishing Co, 1964. p. 110–78.

[19] Bieniawski ZT. Mechanism of brittle rock fracture. Part I: the-

ory of the fracture process. Int J Rock Mech Min Sci Geomech Abstr 1967;4(4):395–406.
[20] Hoek E, Bieniawski ZT. Brittle fracture propagation in rock under compression. Int J Fracture Mech 1965;1(3):137–55.
[21] Lajtai EZ. A theoretical and experimental evaluation of the Griffith theory of brittle fracture. Tectonophysics 1971;11:129–56.
[22] Peng S, Johnson AM. Crack growth and faulting in cylindrical specimens of Chelmsford granite. Int J Rock Mech Min Sci Geomech Abstr 1972;9(1):37–86.
[23] Huang J, Wang Z, Zhao Y. The development of rock fracture from microfracturing to main fracture formation. Int J Rock Mech Min Sci Geomech Abstr 1993;30(7):925–8.
[24] Hatzor YH, Palchik V. The influence of grain size and porosity on crack initiation stress and critical flaw length in dolomites. Int J Rock Mech Min Sci 1997;34(5):805–16.
[25] Lajtai EZ, Dzik EJ. Searching for the damage threshold in intact rock. In: Proceedings of the 2nd North American Rock Mechanics Symposium: Rock Mechanics Tools and Techniques, Montreal. Rotterdam: A.A. Balkema, 1996. p. 701–8.
[26] Eberhardt E, Stead D, Stimpson B, Read R. Changes in acoustic event properties with progressive fracture damage. Int J Rock Mech Min Sci 1997;34(3–4):633.
[27] Brown ET. Rock characterization testing and monitoring: ISRM suggested methods. Oxford: Pergamon Press, 1981.
[28] Martin CD. 17th Canadian Geotechnical Colloquium: the effect of cohesion loss and stress path on brittle rock strength. Can Geotech J 1997;34(5):698–725.
[29] Itasca. FLAC: fast Lagrangian analysis of continua, version 3.3. Minneapolis: Itasca Consulting Group, 1995.
[30] Holcomb DJ, Stone CM, Costin LS. Combining acoustic emission locations and a microcrack damage model to study development of damage in brittle materials. In: Rock mechanics and challenges: Proceedings of the 31st US Symposium, Golden. Rotterdam: A.A. Balkema, 1990. p. 645–51.
[31] Eberhardt E, Stead D, Stimpson B, Lajtai EZ. The effect of neighbouring cracks on elliptical crack initiation and propagation in uniaxial and triaxial stress fields. Eng Fract Mech 1998;59(2):103–15.